Rapid Communications

# $NH_3$ on anatase $TiO_2(101)$: Diffusion mechanisms and the effect of intermolecular repulsion

Kræn C. Adamsen,[1] Esben L. Kolsbjerg,[2] Stig Koust,[1] Lutz Lammich,[1] Bjørk Hammer,[2] Stefan Wendt,[1,*] and Jeppe V. Lauritsen[1,*]

[1]*Interdisciplinary Nanoscience Center (iNANO), Aarhus University, DK-8000 Aarhus C, Denmark*

[2]*Department of Physics and Astronomy, Aarhus University, DK-8000 Aarhus C, Denmark*

(Received 6 July 2020; accepted 13 November 2020; published 1 December 2020)

We utilized scanning tunneling microscopy (STM) experiments and density functional theory (DFT) calculations to study the diffusion of ammonia ($NH_3$) on anatase $TiO_2(101)$. From time-lapsed STM imaging, we observed monomeric and dimeric diffusion channels, and a general tendency to higher diffusion rates with increasing $NH_3$ coverage. In surface regions where several $NH_3$ molecules are adsorbed within a few sites, we further observed the diffusion of $NH_3$ molecules occurring in cascades, where the diffusion of one adsorbate triggers that of others. This eventually leads to apparent diffusion barriers that are lower than expected within a single-jump model. From the DFT calculations, we obtained mechanistic insights into the two observed $NH_3$ diffusion channels. Within the dimeric $NH_3$ diffusion channel, one $NH_3$ swings around another adsorbed $NH_3$ and experiences a reduced diffusion barrier, owing to the intermolecular bonding during the event.

DOI: 10.1103/PhysRevMaterials.4.121601

Titania ($TiO_2$) has numerous actual and potential applications in heterogeneous catalysis, sensors, photovoltaics, and solar-driven hydrogen production [1–3]. To improve the photoresponse of $TiO_2$, doping with nitrogen is a promising approach [4]. In this connection, the interactions of ammonia ($NH_3$) with various $TiO_2$ materials have been studied extensively [5–8]. The interaction of $NH_3$ with $TiO_2$ is also important for an improved understanding of selective catalytic reduction (SCR) catalysis to remove $NO_x$ from exhaust gases [9,10] as well as the removal of $NH_3$ pollution from air and water [11].

Previous surface science studies of $NH_3$ on oxides have focused on the interaction with various rutile $TiO_2$ ($r$-$TiO_2$) surfaces [8,12–17]. These studies revealed that $NH_3$ adsorbs molecularly on $r$-$TiO_2$ surfaces, and $NH_3$ molecules are bound via their lone pairs to fivefold coordinated Ti (5f-Ti) atoms. Even $r$-$TiO_2(110)$ surfaces with surface O vacancies do not lead to $NH_3$ dissociation [17]. Desorption energies were found to decrease from ∼1.1 to 1.3 eV at low $NH_3$ coverage to ∼0.6 eV at full monolayer (ML) coverage [14,17]. This coverage effect was traced back to repulsive $NH_3 - NH_3$ interactions [13,15,17].

Addressing the interaction of $NH_3$ with the technologically more relevant anatase $TiO_2$ ($a$-$TiO_2$), we recently reported about $NH_3$ adsorption on the most abundant (101) face [18]. The $a$-$TiO_2(101)$ surface is well studied, and its interactions with a number of other relevant molecules have been investigated [19–23]. The $a$-$TiO_2(101)$ surface is characterized by a sawtoothlike structure with ridges of twofold coordinated, bridging O atoms ($O_{br}$) along the ⟨010⟩ directions [19]. In addition to 5f-Ti sites, sixfold (fully) coordinated Ti sites (6f-Ti) also exist. Our previous study on $NH_3$ adsorption on $a$-$TiO_2(101)$ revealed that isolated $NH_3$ molecules bind with an adsorption energy of ∼1.2 eV to the 5f-Ti sites [18]. This $NH_3$ adsorption strength is weakened by ∼0.28 eV as the coverage is increased to one ML (one ML is defined as the number of 5f-Ti sites, $5.16\times10^{14}\mathrm{cm}^{-2}$) [18], revealing strong repulsive interactions between $NH_3$ molecules on $a$-$TiO_2(101)$.

So far, scanning tunneling microscopy (STM) studies addressing the diffusion of $NH_3$ barely exist. A low-temperature STM study reported on the motion of $NH_3$ molecules on Cu(100) induced by inelastic tunneling electrons [24], and STM diffusion studies on oxide surfaces have yet to be reported. Here, we use a combination of STM and density functional theory (DFT) to study the thermally activated diffusion of $NH_3$ on $a$-$TiO_2(101)$. In some regions on the $a$-$TiO_2(101)$ surface, we found cascadelike diffusion of $NH_3$ molecules that originates from $NH_3 - NH_3$ repulsion, as well as fast adsorbate diffusion as $NH_3$ dimers. As a result, the measured $NH_3$ hopping rates in these surface regions are greater than expected within a single-jump model. By means of DFT calculations, we unravel how $NH_3$ monomers and $NH_3$ dimers diffuse on $a$-$TiO_2(101)$.

First, we discuss STM experiments [for experimental details, see the Supplemental Material (SM) [25]] conducted at room temperature (RT). The $a$-$TiO_2(101)$ surface was exposed to $NH_3$ and subsequently inspected by STM. As shown in Figs. 1(a) and 1(b), $NH_3$ exposure at RT led to the appearance of isolated bright protrusions that are homogeneously distributed on the surface. These protrusions are ∼1.2 Å high and appear in between the $O_{br}$ rows. This is consistent with the predicted adsorption sites of $NH_3$ molecules being the 5f-Ti sites, and we assigned them to $NH_3$ molecules [18]. The $NH_3$ molecules appear in most instances as well-separated, isolated species. Specifically, they rarely occupy neighboring sites, which is consistent with the reported repulsion between $NH_3$

*Corresponding authors: swendt@phys.au.dk, jvang@inano.au.dk

 

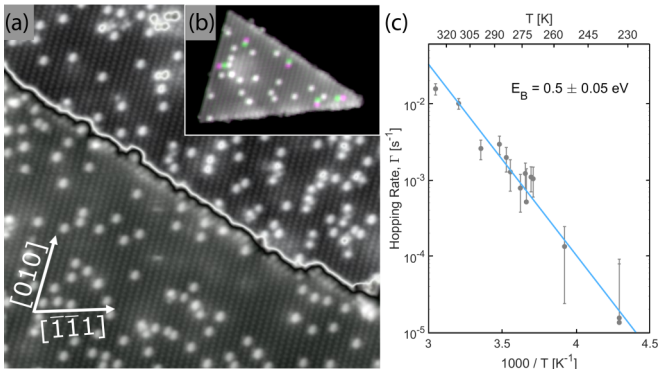


FIG. 1. (a) STM image (300 Å×300 Å; $V_S = +1.0V$; $I_T = 0.1nA$; RT) of the $a$-$TiO_2$(101) surface recorded following $NH_3$ exposure at RT. A repeated grayscale is used for the presentation of this image. The bright features on the terraces arise from $NH_3$ molecules. (b) Superposition of two sequential STM images from an STM movie (200 Å×200 Å) recorded within the same experiment. White protrusions are stationary $NH_3$ molecules. Five $NH_3$ diffusion events occurred: Diffused $NH_3$ molecules in the first (second) STM image are shown in green (pink). (c) Arrhenius plot of the $NH_3$ hopping rate Γ. For each point, we recorded STM movies and analyzed sequences of 50–100 STM images. The $NH_3$ coverage was 0.04–0.06 ML.

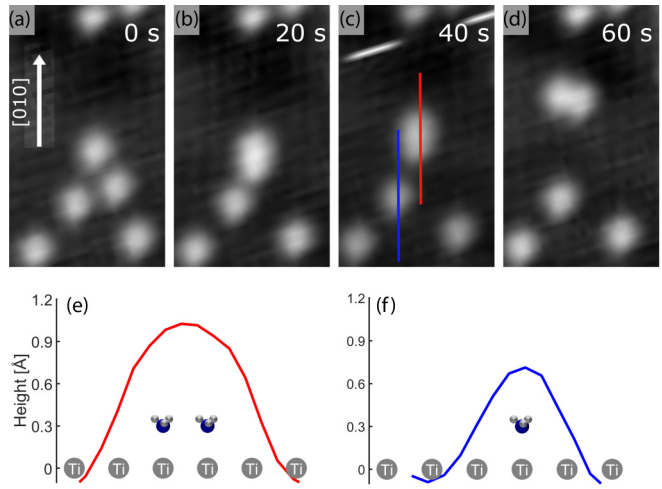


FIG. 2. (a)–(d) Sequence of STM images recorded at 130 K (50 Å×100 Å; 20 s/image), showing the formation, (a)→(b), diffusion, (b)→(c), and breakup, (c)→(d), of an $NH_3$ dimer. (e), (f) STM height profiles along the lines drawn in (c). The profiles of an (e) $NH_3$ dimer and (f) $NH_3$ monomer are shown in red and blue, respectively. Within the dimer, two $NH_3$ molecules occupy nearest-neighbor 5f-Ti sites.

molecules [13,15,17,18]. The $NH_3$ coverage on this sample was ∼0.05 ML, as found by analysis of the STM images.

Imaging the same area repetitively with rates up to three images per minute allowed us to record so-called STM movies. Movie M1 (see SM [25]) was recorded at RT and displays an apparent $NH_3$ hopping rate of $\sim 1\times10^{-3}s^{-1}$. As an example, Fig. 1(b) shows two overlapped consecutive images of Movie M1. In case there is no difference between the two images, the protrusions are presented in grayscale. Hopping events are indicated by color coding, whereby the original protrusion is shown in green and the new protrusion in pink (after the hopping event). In the presented example, there are five hopping events, three of them showing diffusion parallel to the $O_{br}$ rows (in the ⟨010⟩ direction), and two across the $O_{br}$ rows (in the ⟨111⟩ direction).

Because of the low $NH_3$ coverage of 0.04–0.06 ML, it was possible to trace the diffusion of individual $NH_3$ molecules. By marking all molecules in Movie M1 and obtaining their coordinates, we extracted the number of hopping events (frequency) and the total lengths of the diffusion path of each traced $NH_3$ molecule. The two dominating diffusion distances are 3.6 and 5.2 Å (shown in Fig. S1), which matches with the lattice distances along the ⟨010⟩ and ⟨111⟩ directions (parallel to and across the $O_{br}$ rows, respectively). These two distances occur with nearly identical frequencies, indicating similar barriers for hopping in ⟨010⟩ and ⟨111⟩ directions.

To extract information on the $NH_3$ diffusion barrier, we studied $NH_3/a$-$TiO_2$(101) samples at temperatures between 233 and 328 K by recording STM movies. In this temperature range, the diffusion is dominated by single jumps, and it was possible to trace the diffusion pathways of individual $NH_3$ molecules. In an automated analysis process described in the SM [25], the $NH_3$ molecules were marked in the STM movies and their coordinates recorded. For the Arrhenius plot presented in Fig. 1(c), we used the hopping rate Γ [$s^{-1}$] regardless of the specific direction of the diffusion, i.e., we assumed that the diffusion barriers are identical in the ⟨010⟩ and ⟨111⟩ directions. This analysis yielded an energy barrier $E_b$ of $0.5 \pm 0.05$ eV and a preexponential factor (attempt frequency) $\nu_0$ of $t10^6 s^{-1}$ [29].

To further study the diffusion of $NH_3$ on $a$-$TiO_2$(101), we lowered the temperature to 130 K, where single-jump hopping events are nearly frozen out. Surprisingly, we found evidence for rapid $NH_3$ diffusion through the formation of $NH_3$ dimers (see Fig. 2 and Movie M2 [25]). Previously, $NH_3$ dimer formation has been observed on Ru(0001) [30], but the diffusion of $NH_3$ dimers has yet to be investigated. In the lower part of the STM image depicted in Fig. 2(a), five separate monomeric $NH_3$ species can be seen. In the following STM image recorded within this movie [Fig. 2(b)], this situation changed such that two of the five $NH_3$ monomers formed a dimer—see the somewhat brighter protrusion close to the center of the STM image. Consider also that now only four species are located in this area. The newly created $NH_3$ dimer diffuses along the $O_{br}$ row in the [0$\bar{1}$0] direction several lattice distances [see Figs. 2(b) and 2(c)]. Finally, in Fig. 2(d), we again find five $NH_3$ monomers; thus, the $NH_3$ dimer dissociated into two $NH_3$ monomers. The two (new) $NH_3$ monomers close to the center in Fig. 2(d) are adsorbed farther away from the three stationary $NH_3$ monomers. The line profiles presented in Figs. 2(e) and 2(f) show that the $NH_3$ dimer is characterized by a larger STM height than the $NH_3$ monomer. In addition, we illustrate in Fig. 2(e) that $NH_3$ dimers form within the 5f-Ti rows along the ⟨010⟩ directions and that they are centered between two 5f-Ti sites. Note that diffusion of $NH_3$ dimers along the [$\bar{1}\bar{1}$1] direction (across the $O_{br}$ rows) was not observed.

To model the two experimentally identified diffusion modes, we utilized DFT calculations (see SM [25] for details)

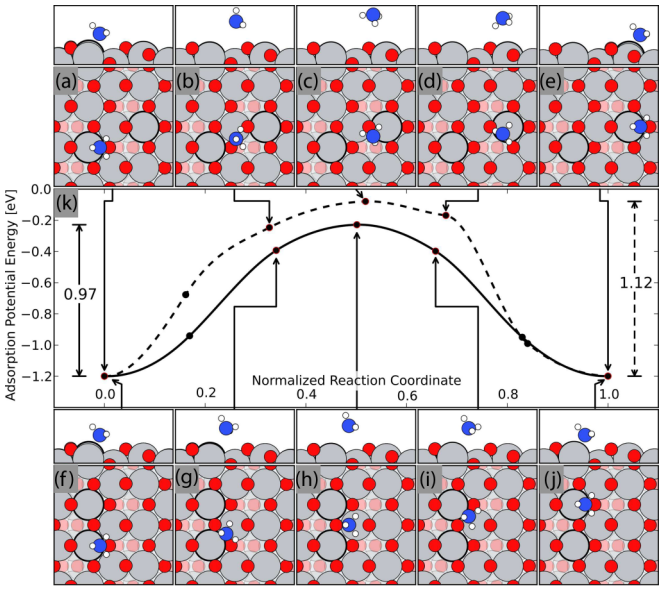


FIG. 3. DFT modeling of monomeric $NH_3$ diffusion. (a)–(e) Pathway across the $O_{br}$ rows: Side and top views are shown. Surface O atoms (small red balls), bulk O atoms (small light red balls), and surface Ti atoms (large gray balls) are indicated. The initial and final 5f-Ti adsorption sites are highlighted by black circles. (f)–(j) Pathway parallel to the $O_{br}$ rows. Presentation of the structures as in (a)–(e). (k) Corresponding energy landscapes. Diffusion pathways across (dashed line) and parallel to the $O_{br}$ rows (solid line) are directly compared. Arrows point to the corresponding computed energies.

using a fully stoichiometric $a$-$TiO_2(101)$ slab consisting of four $TiO_2$ trilayers, spanning $1\times2$ surface unit cells. We used the ASE package (ASE = atomic simulation environment) [31] in combination with the GPAW [32] DFT code. We employ the optB88-vdW functional [33] which is known to describe both hydrogen bonds and more dispersive interactions well.

Addressing monomeric $NH_3$ diffusion, Figs. 3(a)–3(e) shows the most favorable pathway for diffusion along the $[\bar{1}\bar{1}1]$ direction, and Figs. 3(f)–3(j) illustrate the most favorable diffusion pathway along the $[0\bar{1}0]$ direction (parallel to the $O_{br}$ rows). In each case, the initial and final 5f-Ti adsorption sites are marked by black circles. The corresponding energy landscapes are presented in Fig. 3(k).

In the case of diffusion of an $NH_3$ molecule across the $O_{br}$ rows (along the $[\bar{1}\bar{1}1]$ direction) [see Figs. 3(a)–3(e)], one of the H atoms of the $NH_3$ molecule forms a hydrogen bond to the $O_{br}$ that is crossed [Fig. 3(b)]. Because of this, the $NH_3$ lone pair points into the vacuum [Figs. 3(c) and 3(d)] instead of to the surface, as is the case when adsorbed on a regular 5f-Ti adsorption site. Subsequently, the $NH_3$ molecule rolls over the $O_{br}$ atom [Figs. 3(c) and 3(d)] before it reaches the next 5f-Ti site [Fig. 3(e)]. As can be seen in Fig. 3(k), this diffusion pathway is characterized by an energy barrier of 1.12 eV (dashed curve). The weakest bonding occurs when the $NH_3$ molecule rolls over the $O_{br}$ atom [Fig. 3(c)].

In the case of $NH_3$ monomer diffusion *parallel* to the $O_{br}$ rows (along the $[0\bar{1}0]$ direction) [see Figs. 3(f)–3(j)], the $NH_3$ molecule prefers a slightly curved pathway via the neighboring fully coordinated 6f-Ti site [Fig. 3(h)]. No "rollover" occurs within this pathway. The $NH_3$ molecule is weakest bound when it passes the 6f-Ti site [Fig. 3(h)]. We found a barrier of 0.97 eV [see the solid curve in Fig. 3(k)], which is slightly lower than the one computed for $NH_3$ diffusion across the $O_{br}$ row.

We further modeled the diffusion of $NH_3$ dimers on $a$-$TiO_2(101)$ (see Fig. 4). Once formed, $NH_3$ dimers are very diffusive in the $[0\bar{1}0]$ direction (parallel to the $O_{br}$ rows), as evidenced by the experimental observation of such movements at low temperatures (see Fig. 2). We identified two possible $NH_3$ dimer diffusion pathways in the $[0\bar{1}0]$ direction. In the starting configuration, two $NH_3$ molecules are adsorbed at neighboring 5f-Ti sites [Figs. 4(a) and 4(e)]. In each case, one $NH_3$ molecule stays adsorbed on its 5f-Ti site, while the second molecule is moving either "left" [Figs. 4(a)–4(d)] or "right" [Figs. 4(e)–4(h)] around the stationary $NH_3$ molecule. The stationary $NH_3$ molecule solely rotates and slightly shifts its position.

In case of the pathway right around the stationary $NH_3$ molecule, the moving $NH_3$ molecule tilts and forms a hydrogen bond to the stationary $NH_3$ molecule [see Fig. 4(b)]. The hydrogen bound $NH_3$ dimer can then rotate around the 5f-Ti site at which the stationary $NH_3$ molecule is adsorbed [Figs. 4(b) and 4(c)]. Finally, the moving $NH_3$ molecule has reached the 5f-Ti site on the other side of the stationary $NH_3$ molecule [Fig. 4(d)], i.e., the $NH_3$ dimer has diffused one lattice space in the $[0\bar{1}0]$ direction. As shown in Fig. 4(j) (dashed curve), this diffusion pathway is characterized by a barrier of 0.82 eV. The diffusion pathway left around the stationary $NH_3$ molecule [Figs. 4(e)–4(h)] proceeds analogously to the pathway right around the stationary $NH_3$ molecule. The computed diffusion barrier [see Fig. 4(j) (solid curve)] is with 0.75 eV a little lower than that for diffusion right around the stationary $NH_3$ molecule. For a direct comparison, Fig. 4(i) shows the two identified dimer diffusion pathways together (top view). In agreement with the experimental observations, we found by DFT modeling that $NH_3$ dimer diffusion is more facile than $NH_3$ monomer diffusion ($0.75-0.82$ eV vs $0.97-1.12$ eV. This difference of the diffusion barriers is related to a strong hydrogen bond that forms upon diffusion between the two $NH_3$ within the dimer [34].

Comparing the experimental diffusion data presented in Fig. 1(c) with the computed diffusion barriers (Figs. 3 and 4), there seems to be a contradiction. Even if dimer diffusion would be entirely dominating, there is a difference of at least 0.25 eV between the experimentally (0.50 eV) and any of the theoretically deduced diffusion barriers. We attribute this difference (i) to repulsive interactions between adsorbed $NH_3$ molecules that become increasingly important when many $NH_3$ molecules are adsorbed in close proximity, and (ii) to the approximations made in the DFT simulations (see SM [25]).

We observed clear examples of repulsive interactions between adsorbed $NH_3$ molecules in STM movies recorded at RT, one of which is illustrated in Figs. 5(a)–5(f). Specifically, we found that $NH_3$ molecules are hopping much more frequently if their distances to each other are smaller than $10-13$ Å (see Fig. S2). In Fig. 5(a), five separated $NH_3$ molecules are seen in the scanned area on $a$-$TiO_2(101)$. Before the acquisition of this STM image, the imaged five $NH_3$ molecules did not move for ~120 s. Thus, at these specific

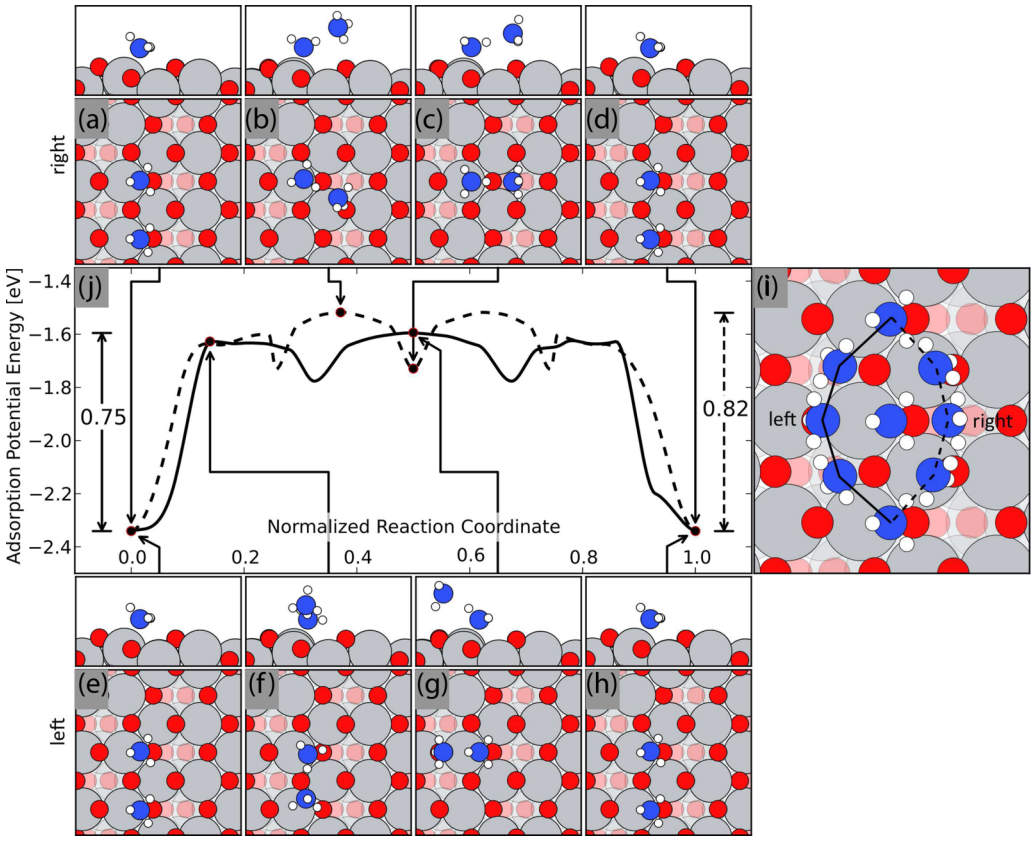


FIG. 4. DFT modeling of dimeric $NH_3$ diffusion parallel to the $O_{br}$ rows. (a)–(d) The moving $NH_3$ molecule takes the pathway on the right around the stationary $NH_3$ molecule. Side and top views are shown. Presentation of the structures as in Fig. 3. (e)–(h) The moving $NH_3$ molecule takes the pathway on the left around the stationary $NH_3$ molecule. (i) Direct comparison of the two pathways (top view). (j) Diffusion energy landscapes. Dashed and solid lines correspond to the pathways on the right and left around the stationary $NH_3$ molecule, respectively. Arrows point to the corresponding computed energies.

adsorption sites, the nearest-neighbor distances between the $NH_3$ molecules (∼12 Å and larger) were favorable (no strong repulsion). Then, suddenly three of the five $NH_3$ molecules diffused several lattice distances [see Fig. 5(b)]. Presumably, a single diffusion event has occurred that triggered the diffusion of the other $NH_3$ molecules (diffusion in cascades). Following

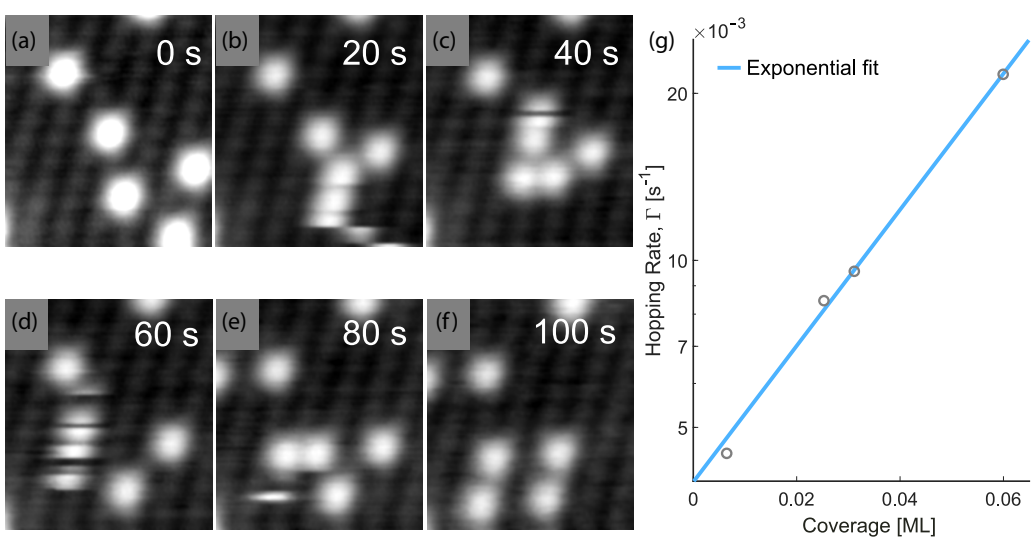


FIG. 5. (a)–(f) Sequence of STM images (40 Å×50 Å; 20 s/image) showing "cascade diffusion" of five $NH_3$ molecules at RT. The imaged five $NH_3$ molecules did not hop within 120 s (six images) prior to the image shown in (a). From image (a) to image (b), several hopping events occurred, and this cascade of hopping events of neighboring $NH_3$ molecules continued for ∼100 s until in image (f), the five molecules reached an arrangement that persisted for four images (∼80 s). (g) Hopping rate at RT as a function of the $NH_3$ coverage.

this, several further diffusion events were observed, leading to the different configurations in Figs. 5(c)–5(e), until the $NH_3$ molecules eventually settled in a new configuration [Fig. 5(f)] where all molecules are well separated. No diffusion occurred during the following 80 s.

To evaluate the influence of $NH_3$ coverage on the diffusion quantitatively, we recorded several STM movies at RT on samples where the coverage varied between 0.005 and 0.05 ML [see Fig. 5(g)]. The results show that the hopping rate $\Gamma$ increases exponentially with increasing $NH_3$ coverage (notice the logarithmic scale). We explain this pronounced coverage effect on $NH_3$ diffusion by repulsion between $NH_3$ molecules. Accordingly, for a meaningful comparison of experimentally observed diffusion data with the computed diffusion barriers, the $NH_3$ coverages in the experiments must be very low. As soon as $NH_3 - NH_3$ repulsion comes into play, $\Gamma$ increases because adsorbate arrangements with $NH_3 - NH_3$ distances larger than ∼10–13 Å are clearly preferred. Our diffusion data summarized in Fig. 1(c) represent the collective measurement of thermally activated single-jump diffusion *and* diffusion events induced by repulsion.

For comparison, we also studied the diffusion of water dimers on $a$-$TiO_2(101)$ (see Fig. S3). Fast diffusion of water dimers has been observed on Pd(111) [35], several other metallic surfaces (see Ref. [36] and references therein), and on rutile $TiO_2(110)$ [37]. Indeed, we also observed the formation of water dimers on $a$-$TiO_2(101)$ [25], and we find similarities between the diffusion behaviors of water and $NH_3$. As found for $NH_3$, the water dimers diffuse faster than monomers, and dimer diffusion occurs exclusively parallel to the $O_{br}$ rows. The latter resembles the situation for water on rutile $TiO_2(110)$. However, the water dimers on rutile $TiO_2(110)$ are quite stable [37], whereas the dimers on $a$-$TiO_2(101)$ split frequently again into monomers (see Fig. S3). Interestingly, the $NH_3$ dimers on $a$-$TiO_2(101)$ are very short lived, too. Extending these findings, we believe that the diffusion of H-bonded molecule clusters on a selected surface resemble each other irrespectively of the specific adsorbate.

In summary, we utilized high-resolution STM and DFT calculations to study the diffusion of $NH_3$ on anatase $TiO_2(101)$. Via recording STM movies and conducting an Arrhenius analysis, we found an apparent diffusion barrier of ∼0.5 eV at 0.05 ± 0.01 ML $NH_3$ coverage. However, even at this low coverage, the diffusion of $NH_3$ can be affected by repulsive adsorbate interactions. In addition, we uncovered monomeric and dimeric $NH_3$ diffusion channels via STM. Short-lived $NH_3$ dimers form on the surface despite the repulsion between the $NH_3$ monomers. The $NH_3$ dimers diffuse clearly faster than the $NH_3$ monomers. Our DFT simulations provide detailed mechanistic insights into the $NH_3$ diffusion. In qualitative agreement with the STM experiments, the $NH_3$ dimer pathways are characterized by barriers that are ∼0.22 eV lower in energy than the ones computed for $NH_3$ monomers (of ∼1.0 eV). We anticipate that the gained knowledge on the diffusion of $NH_3$ on anatase $TiO_2(101)$ is useful for an understanding of the diffusion of $NH_3$ and other hydrogen-bonded adsorbates on oxide surfaces in general.

We acknowledge support from the Innovation Fund Denmark (IFD), File No. 6151-00008B (ProNOx), the Villum Fonden (Investigator grant, Project No. 16562), and Haldor Topsoe A/S.

[1] M. Grätzel, Dye-sensitized solar cells, J. Photochem. Photobiol. C **4**, 145 (2003).

[2] U. Diebold, The surface science of titanium dioxide, Surf. Sci. Rep. **48**, 53 (2003).

[3] X. Chen and S. S. Mao, Titanium dioxide nanomaterials: Synthesis, properties, modifications, and applications, Chem. Rev. **107**, 2891 (2007).

[4] R. Asahi, T. Morikawa, T. Ohwaki, K. Aoki, and Y. Taga, Visible-light photocatalysis in nitrogen-doped titanium oxides, Science **293**, 269 (2001).

[5] O. Diwald, T. L. Thompson, T. Zubkov, E. G. Goralski, S. D. Walck, and J. T. Yates Jr., Photochemical activity of nitrogen-doped rutile $TiO_2(110)$ in visible light, J. Phys. Chem. B **108**, 6004 (2004).

[6] R. P. Vitiello, J. M. Macak, A. Ghicov, H. Tsuchiya, L. F. P. Dick, and P. Schmuki, N-Doping of anodic $TiO_2$ nanotubes using heat treatment in ammonia, Electrochem. Commun. **8**, 544 (2006).

[7] J. Wang, D. N. Tafen, J. P. Lewis, Z. L. Hong, A. Manivannan, M. J. Zhi, M. Li, and N. Q. Wu, Origin of photocatalytic activity of nitrogen-doped $TiO_2$ nanobelts, J. Am. Chem. Soc. **131**, 12290 (2009).

[8] Y. K. Kim, S. Park, K. J. Kim, and B. Kim, Photoemission study of N-doped $TiO_2(110)$ with $NH_3$, J. Phys. Chem. C **115**, 18618 (2011).

[9] G. Busca, L. Lietti, G. Ramis, and F. Berti, Chemical and mechanistic aspects of the selective catalytic reduction of $NO_x$ by ammonia over oxide catalysts: A review, Appl. Catal. B **18**, 1 (1998).

[10] I. E. Wachs, Catalysis science of supported vanadium oxide catalysts, Dalton Trans. **42**, 11762 (2013).

[11] S. Yamazoe, T. Okumura, Y. Hitomi, T. Shishido, and T. Tanaka, Mechanism of photo-oxidation of $NH_3$ over $TiO_2$: Fourier transform infrared study of the intermediate species, J. Phys. Chem. C **111**, 11077 (2007).

[12] E. L. Roman, J. L. Desegovia, R. L. Kurtz, R. Stockbauer, and T. E. Madey, UPS synchrotron radiation studies of $NH_3$ adsorption on $TiO_2(110)$, Surf. Sci. **273**, 40 (1992).

[13] U. Diebold and T. E. Madey, Adsorption and electron-stimulated desorption of $NH_3/TiO_2(110)$, J. Vac. Sci. Technol. A **10**, 2327 (1992).

[14] E. Farfan-Arribas and R. J. Madix, Characterization of the acid-base properties of the $TiO_2(110)$ surface by adsorption of amines, J. Phys. Chem. B **107**, 3225 (2003).

[15] J. N. Wilson and H. Idriss, Reactions of ammonia on stoichiometric and reduced $TiO_2(001)$ single crystal surfaces, Langmuir **20**, 10956 (2004).

[16] C. L. Pang, A. Sasahara, and H. Onishi, Scanning tunnelling microscopy study of ammonia adsorption on $TiO_2(110)$, Nanotechnology **18**, 4 (2007).

[17] B. Kim, Z. J. Li, B. D. Kay, Z. Dohnalek, and Y. K. Kim, The effect of oxygen vacancies on the binding interactions of $NH_3$ with rutile $TiO_2$(110)-1×1, Phys. Chem. Chem. Phys. **14**, 15060 (2012).

[18] S. Koust, K. C. Adamsen, E. L. Kolsbjerg, Z. Li, B. Hammer, S. Wendt, and J. V. Lauritsen, $NH_3$ adsorption on anatase-$TiO_2$(101), J. Chem. Phys. **148**, 5 (2018).

[19] U. Diebold, N. Ruzycki, G. S. Herman, and A. Selloni, One step towards bridging the materials gap: surface studies of $TiO_2$ anatase, Catal. Today **85**, 93 (2003).

[20] Y. B. He, A. Tilocca, O. Dulub, A. Selloni, and U. Diebold, Local ordering and electronic signatures of submonolayer water on anatase $TiO_2$(101), Nat. Mater. **8**, 585 (2009).

[21] D. C. Grinter, M. Nicotra, and G. Thornton, Acetic acid adsorption on anatase $TiO_2$(101), J. Phys. Chem. C **116**, 11643 (2012).

[22] M. Setvin, B. Daniel, U. Aschauer, W. Hou, Y. F. Li, M. Schmid, A. Selloni, and U. Diebold, Identification of adsorbed molecules via STM tip manipulation: CO, $H_2O$ and $O_2$ on $TiO_2$ anatase (101), Phys. Chem. Chem. Phys. **16**, 21524 (2014).

[23] M. Setvin, M. Buchholz, W. Y. Hou, C. Zhang, B. Stoger, J. Hulva, T. Simschitz, X. Shi, J. Pavelec, G. S. Parkinson, M. C. Xu, Y. M. Wang, M. Schmid, C. Wöll, A. Selloni, and U. Diebold, A multitechnique study of CO adsorption on the $TiO_2$ anatase (101) surface, J. Phys. Chem. C **119**, 21044 (2015).

[24] J. I. Pascual, N. Lorente, Z. Song, H. Conrad, and H.-P. Rust, Selectivity in vibrationally mediated single-molecule chemistry, Nature (London) **423**, 525 (2003).

[25] See Supplemental Material at http://link.aps.org/supplemental/10.1103/PhysRevMaterials.4.121601 for Movies M1 and M2, experimental and computational details, the automated analysis process of the STM images (movies), diffusion distances extracted from Movie M1, histograms of moved and stationary $NH_3$ molecules at RT, the influence of the approximations made in the DFT simulations, and the diffusion of water dimers on *a*-$TiO_2$(101), which includes Refs. [26–28].

[26] S. Koust, L. Arnarson, P. G. Moses, Z. Li, I. Beinik, J. V. Lauritsen, and S. Wendt, Facile embedding of single vanadium atoms at the anatase $TiO_2$(101) surface, Phys. Chem. Chem. Phys. **19**, 9424 (2017).

[27] G. Goubert, Y. Dong, M. N. Groves, J. C. Lemay, B. Hammer, and P. H. McBreen, Monitoring interconversion between stereochemical states in single chirality-transfer complexes on a platinum surface, Nat. Chem. **9**, 531 (2017).

[28] E. L. Kolsbjerg, M. N. Groves, and B. Hammer, An automated nudged elastic band method, J. Chem. Phys. **145**, 9 (2016).

[29] Compared to reported values for NH/$r$−TiO(110) [15,17], this preexponential factor is unusually low. We have carefully checked our data for possible reasons for this surprising result. For example, we tested whether $NH_3$ diffusion in cascades described below is a possible reason. The exact origin of the low preexponential factor needs further exploration.

[30] S. Maier, I. Stass, J. I. Cerda, and M. Salmeron, Bonding of ammonia and its dehydrogenated fragments on Ru(0001), J. Phys. Chem. C **116**, 25395 (2012).

[31] A. H. Larsen, J. J. Mortensen, J. Blomqvist, I. E. Castelli, R. Christensen, M. Dulak, J. Friis, M. N. Groves, B. Hammer, C. Hargus *et al.*, The atomic simulation environment-a Python library for working with atoms, J. Phys.: Condens. Matter **29**, 30 (2017).

[32] J. Enkovaara, C. Rostgaard, J. J. Mortensen, J. Chen, M. Dulak, L. Ferrighi, J. Gavnholt, C. Glinsvad, V. Haikola, H. A. Hansen *et al.*, Electronic structure calculations with GPAW: A real-space implementation of the projector augmented-wave method, J. Phys.: Condens. Matter **22**, 253202 (2010).

[33] J. Klimes, D. R. Bowler, and A. Michaelides, Chemical accuracy for the van der Waals density functional, J. Phys.: Condes. Matter **22**, 5 (2010).

[34] The strong hydrogen bond between the NH molecules in the dimer leads to a relatively strong bond of the moving NH molecule and a low dimer diffusion barrier. In contrast, in case of $NH_3$ monomer diffusion, the $NH_3$ molecule experiences its weakest bonding when it is bound either to the $O_{br}$ atom through its hydrogens, leaving its lone pair pointing into the vacuum, or to the fully coordinated 6f-Ti site via its lone pair. In these configurations, the $NH_3$ molecule is very loosely bound, resulting in high diffusion barriers that are close to the desorption energy (1.2 eV).

[35] S. Mitsui, M. K. Rose, E. Fromin, D. F. Ogletree, and M. Salmeron, Water diffusion and clustering on Pd(111), Science **297**, 1850 (2002).

[36] W. Fang, J. Chen, P. Pedevilla, X.-Z. Li, J. O. Richardson, and A. Michaelides, Origins of fast diffusion of water dimers on surfaces, Nat. Commun. **11**, 1689 (2020).

[37] J. Matthiesen, J. Ø. Hansen, S. Wendt, E. Lira, R. Schaub, E. Lægsgaard, F. Besenbacher, and B. Hammer, Formation and Diffusion of Water Dimers on Rutile $TiO_2$(110), Phys. Rev. Lett. **102**, 226101 (2009).